

Efficient Bayesian inference of fully stochastic epidemiological models with applications to COVID-19

Yuting I. Li,¹ Günther Turk,^{1,*} Paul B. Rohrbach,^{1,*} Patrick Pietzonka,^{1,*} Julian Kappler,^{1,*} Rajesh Singh,^{1,*} Jakub Dolezal,^{1,*} Timothy Ekeh,¹ Lukas Kikuchi,¹ Joseph D. Peterson,¹ Austen Bolitho,¹ Hideki Kobayashi,¹ Michael E. Cates,¹ R. Adhikari,¹ and Robert L. Jack^{1,2}

¹*Department of Applied Mathematics and Theoretical Physics,
University of Cambridge, Wilberforce Road, Cambridge CB3 0WA, United Kingdom*

²*Department of Chemistry, University of Cambridge,
Lensfield Road, Cambridge CB2 1EW, United Kingdom*

Epidemiological forecasts are beset by uncertainties in the generative model for the disease, and the surveillance process through which data are acquired. We present a Bayesian inference methodology that quantifies these uncertainties, for epidemics that are modelled by (possibly) non-stationary, continuous-time, Markov population processes. The efficiency of the method derives from a functional central limit theorem approximation of the likelihood, valid for large populations. We demonstrate the methodology by analysing the early stages of the COVID-19 pandemic in the UK, based on age-structured data for the number of deaths. This includes maximum a posteriori estimates, MCMC sampling of the posterior, computation of the model evidence, and the determination of parameter sensitivities via the Fisher information matrix. Our methodology is implemented in PyRoss, an open-source platform for analysis of epidemiological compartment models.

I. INTRODUCTION

The ongoing COVID-19 pandemic has demonstrated the vital importance of epidemiological forecasting [1–6]. Given the large uncertainties in the mechanisms of viral transmission, and the difficulties in determination of numbers of infections and deaths, a Bayesian approach is natural [7–11]. This allows the range of likely outcomes to be quantified and characterised. The evidence in favour of different epidemiological models can also be assessed, in the light of data.

Compartment models are widely used as models of epidemiological dynamics [12–14]. Within these models, individuals are grouped into cohorts, for example according to their age or location. The key assumption is that the rates of contact between individuals depend only on their cohorts. The resulting models have sufficient complexity to be useful in forecasting, while remaining simple enough that Bayesian analyses are tractable [8–10, 15].

Such analyses require three main ingredients: the definition of a model, the prior distributions of the inference parameters, and an efficient method for the evaluation of the posterior distribution [12, 16–20]. In this work, we derive the model likelihood directly from the model definition, via a functional central limit theorem (CLT) [21–25]. Hence, for any given model, the likelihood can be derived by a generic and automated procedure. This enables rapid Bayesian fitting of models to data with fully quantified uncertainties, as implemented in the PyRoss package [26]. It also enables sampling from the posterior by Markov chain Monte Carlo (MCMC), and the evaluation of model evidence [27–29], so that models may be

compared by their posterior probabilities. The results presented here build on an earlier technical report [10] which discussed automated fitting of such models to data.

In any Bayesian calculation of this type, the choice of likelihood function makes assumptions (either implicit or explicit) about the role of random fluctuations in the disease propagation and the surveillance of the epidemic. In the models that we consider, both the disease dynamics and the surveillance (data collection) processes are encapsulated in a single compartment model. It follows that our Gaussian approximation for the likelihood is accurate in the limit where the epidemic is spreading in a large well-mixed population [21–25] – in this sense, it accounts for all sources of stochasticity within the model. Another common approach is to consider a deterministic generative model for the disease, and to treat the data collection (surveillance) as a stochastic process [7, 9, 15, 30]. These approaches have different strengths and weaknesses, which are discussed below.

This article describes the Bayesian methodology that we use, including definitions of the relevant models (Sec. II) and the specification of the data and likelihood (Sec. III). The inference methods are summarised in Sec. IV. As proof of principle for our approach, we perform inference on a compartment model for the COVID-19 epidemic in England and Wales, over the period 6-March to 15-May 2020, using data for the number of deaths. A more detailed picture of the epidemic would be available by combining multiple data sources, but the computation that we present is appropriate as an illustration of the general methodology. We compare several variants of the model, which differ in their assumed contact structure; we also compare the model evidence [27–29] for the different variants. The models are defined in Sec. V, while Sec. VI shows the results. We conclude with a discussion in Sec. VII. Some technical details and

*Contributed equally

supplementary results are provided in appendices.

II. COMPARTMENT MODELS

A. Definition

Consider a compartment model where N individuals are grouped into M cohorts, according to some attributes (for example age and/or gender). Each cohort is divided into L epidemiological classes, indexed by $\ell = 1, 2, \dots, L$. We assume a single susceptible class, which is $\ell = 1$. Other classes may be either infectious or non-infectious: the canonical example is an SIR model which corresponds to $L = 3$, in which case the recovered (R) class is non-infectious.

In the general case, the total number of compartments is $M \times L$ and the state of the system can be specified as a vector

$$\mathbf{n} = (n_1, n_2, \dots, n_{M \times L}) . \quad (1)$$

We use boldface notation throughout this work to indicate both vectors and matrices. Each element of \mathbf{n} is a non-negative integer, such that the number of individuals in class ℓ and cohort i is $n_{i+M(\ell-1)}$. For example n_1, \dots, n_M are the number of susceptible individuals in each cohort.

The disease propagation involves individuals moving between the epidemiological classes, by a Markov population process [31]. (Models may also include immigration or emigration steps where the total population changes.) The parameters of the model are $\boldsymbol{\theta} = (\theta_1, \theta_2, \dots)$, indexed by a label a . The various stochastic transitions are indexed by $\xi = 1, 2, \dots$. In transition ξ , the population \mathbf{n} is updated by a vector \mathbf{r}_ξ with integer elements, that is

$$\mathbf{n} \rightarrow \mathbf{n} + \mathbf{r}_\xi \quad \text{with rate} \quad w_\xi(t, \boldsymbol{\theta}, \mathbf{n}) . \quad (2)$$

For example, if transition ξ involves a single individual moving from compartment α to compartment β then \mathbf{r}_ξ has -1 in the α -th place and $+1$ in the β -th place, with all other elements being zero. Consistent with the Markovian assumption, the rate $w_\xi(t, \boldsymbol{\theta}, \mathbf{n})$ depends on the current state, the parameters of the model, and the time t .

Two common types of transition are infection, and progression from one stage to another. For example, in the simple SIR example (with $M = 1$) we write $(n_1, n_2, n_3) = (S, I, R)$ with total population $N = S + I + R$. Taking infection and recovery parameters as $\boldsymbol{\theta} = (\beta, \gamma)$, the infection transition has $\mathbf{r}_1 = (-1, 1, 0)$ and rate $w_1 = \beta SI/N$, while progression for I to R has $\mathbf{r}_2 = (0, -1, 1)$ and $w_2 = \gamma I$. The general formalism used here covers simple SIR models as well as more complex ones, see for example Sec. V.

B. Contact dynamics and the well-mixed assumption

As illustrated by the SIR example, it is a general feature that progression transitions have rates that are linear in \mathbf{n} , but infections are bilinear. As usual, we consider compartment models that assume a well-mixed population, in the sense that the typical frequency of meetings between individuals depends only on their cohort. These frequencies are described by the *contact matrix* [12–14, 32], which appears in the rates w_ξ for infectious transitions (for an example, see Sec. V below).

This well-mixed assumption neglects the detailed social structure of the population, for example that friends and family members meet each other much more frequently than other individuals. Despite this (coarse) approximation, compartment models are valuable tools for practical analysis of epidemics, and are useful for inference. Still, it must be borne in mind in the following that these models are not microscopically resolved descriptions of individuals' behavior, but rather approximate descriptions that capture the main features of disease dynamics, and its dependence on model parameters.

C. Average dynamics and law of large numbers

We will be concerned with epidemics in large populations, with the well-mixed assumptions described above. The relevant limit is controlled by a large parameter Ω . In models where the total population N is fixed then $\Omega = N$. If the population is uncertain or subject to change then Ω is taken as a suitable reference value, for example the prior mean population at time $t = 0$. Now define

$$\mathbf{x} = \frac{1}{\Omega} \mathbf{n} \quad (3)$$

whose elements indicate the fractions of individuals in each compartment. Within the well-mixed assumption, the rates w_ξ have a specific dependence on Ω :

$$w_\xi(t, \boldsymbol{\theta}, \Omega \mathbf{x}) = \Omega \omega_\xi(t, \boldsymbol{\theta}, \mathbf{x}) \quad (4)$$

where ω_ξ is the transition rate per individual (as opposed to the rate for the population).

Given the parameters $\boldsymbol{\theta}$ and an initial condition $\mathbf{x}(0)$, models of this form obey a law of large numbers in the limit of large population $\Omega \rightarrow \infty$. In this limit, almost all stochastic trajectories $\mathbf{x}(t)$ lie close to a single deterministic trajectory, $\bar{\mathbf{x}}(t)$ [33–36], which can be obtained as the solution of an ordinary differential equation

$$\frac{d\bar{\mathbf{x}}}{dt} = \sum_{\xi} \mathbf{r}_\xi \omega_\xi(t, \boldsymbol{\theta}, \bar{\mathbf{x}}) . \quad (5)$$

The sum in this equation runs over all possible values of ξ ; we do not write the range explicitly in such cases, for compactness of notation. Equ. (5) is straightforwardly solved by numerical methods, so $\bar{\mathbf{x}}$ can be computed.

D. Central limit theorem

The likelihood that we use for Bayesian analysis rests on a functional CLT [21–25] for fluctuations of the epidemiological state about the mean value $\bar{\mathbf{x}}$. This is derived for a fixed initial condition $\mathbf{x}(0)$. To analyse fluctuations, consider the (scaled) deviation of the epidemiological state \mathbf{x} from its average

$$\mathbf{u}(t) = \sqrt{\Omega} [\mathbf{x}(t) - \bar{\mathbf{x}}(t)] \quad (6)$$

with $\mathbf{u}(0) = 0$. (The factor of $\sqrt{\Omega}$ is standard in CLTs, it is chosen so that typical trajectories of the model have \mathbf{u} of order unity, as $\Omega \rightarrow \infty$.) By considering the increment in \mathbf{u} over a short time-interval and taking the limit of large Ω , one finds [37, Sec 4.5.9] that \mathbf{u} obeys a stochastic differential equation

$$d\mathbf{u} = \mathbf{J}(t, \boldsymbol{\theta}, \bar{\mathbf{x}}) \mathbf{u} dt + \sum_{\xi} \boldsymbol{\sigma}_{\xi}(t, \boldsymbol{\theta}, \bar{\mathbf{x}}) dW_{\xi} \quad (7)$$

where W_1, W_2, \dots are independent standard Brownian motions (Wiener processes); our notation suppresses the dependence of $\bar{\mathbf{x}}$ and \mathbf{u} on the time t , for compactness. The elements of the square matrix \mathbf{J} are

$$J_{ij}(t, \boldsymbol{\theta}, \bar{\mathbf{x}}) = \sum_{\xi} r_{\xi,i} \left. \frac{\partial}{\partial x_j} \omega_{\xi}(t, \boldsymbol{\theta}, \mathbf{x}) \right|_{\mathbf{x}=\bar{\mathbf{x}}}, \quad (8)$$

where $r_{\xi,i}$ is the i th element of the vector \mathbf{r}_{ξ} . Similarly,

$$\boldsymbol{\sigma}_{\xi}(t, \boldsymbol{\theta}, \bar{\mathbf{x}}) = \mathbf{r}_{\xi} \sqrt{\omega_{\xi}(t, \boldsymbol{\theta}, \bar{\mathbf{x}})}. \quad (9)$$

In the physics literature, the derivation of (7) uses the van-Kampen expansion [36, 37]; the use of these methods in population dynamics is due to Kurtz [33–35].

One sees that \mathbf{J} and $\boldsymbol{\sigma}_{\xi}$ depend on the deterministic path $\bar{\mathbf{x}}$ but not on the random variable \mathbf{u} , so (7) is a time-dependent Ornstein-Uhlenbeck process. The CLT applies as $\Omega \rightarrow \infty$, it states that \mathbf{u} has Gaussian fluctuations with mean zero, and a covariance that can be derived from (7). This result applies to the covariance at any fixed time, and to correlations between fluctuations at different times. The correlations are discussed in Appendix A, for example (A6,A8).

III. DATA AND LIKELIHOOD

A central task in Bayesian inference is to compute the posterior distribution of the parameters $\boldsymbol{\theta}$, given some observational data. The posterior probability density function (pdf) of the parameters is [16–18]

$$P(\boldsymbol{\theta}|\text{data}) = \frac{P(\text{data}|\boldsymbol{\theta})P(\boldsymbol{\theta})}{Z(\text{data})} \quad (10)$$

where $Z(\text{data})$ is called the model evidence, which is fixed by normalisation of the posterior.

We now describe how the observed data are incorporated in our methodology, after which we discuss the likelihood. A technical aspect of our approach is that the initial condition of the system at time $t = 0$ must be parameterised in terms of $\boldsymbol{\theta}$ (or explicitly provided).

A. Data

In practical situations, observations of the epidemiological state are subject to uncertainty. Our methodology includes all random aspects of the observation (surveillance) process directly into the model. This means that measured data can be identified with the populations of certain model compartments; the remainder of the compartments are not observed, and correspond to latent variables. For example, the model of Sec. V (below) includes an observed compartment for deceased individuals, which should properly be interpreted as a compartment for deceased individuals who were diagnosed with COVID-19. Other compartments – for example susceptible and infected – are latent variables, which are independent of diagnosis. The measurement process is then modelled through the (stochastic) transition from infected compartment to deceased compartment, whose rate depends on the probability of correct diagnosis.

We assume that observations are made at an ordered set of positive times, indexed by $\mu = 1, 2, \dots$. Specifically, at time t_{μ} , one observes a vector with m_{obs} elements, which are linear combinations of the compartment populations at that time. That is,

$$\mathbf{n}^{\text{obs}}(t_{\mu}) = \mathbf{F} \mathbf{n}(t_{\mu}) \quad (11)$$

where \mathbf{F} is a matrix of size $m_{\text{obs}} \times (ML)$, which we call the *filter matrix*.

Now define a vector \mathbf{Y} that contains all the observed data, by collecting the individual observation vectors:

$$\mathbf{Y} = (\mathbf{n}^{\text{obs}}(t_1), \mathbf{n}^{\text{obs}}(t_2), \dots). \quad (12)$$

This vector corresponds to the data in (10).

B. Likelihood

The likelihood is denoted by

$$\mathcal{L}(\boldsymbol{\theta}) = P(\mathbf{Y}|\boldsymbol{\theta}). \quad (13)$$

Hence we require a computationally tractable estimate of this probability. The formula that we use is based on the CLT for the path $\mathbf{x}(t)$, as discussed in Sec. IID.

Given the parameters $\boldsymbol{\theta}$, the most likely observation is $\bar{\mathbf{Y}}$, whose elements are

$$\bar{\mathbf{n}}^{\text{obs}}(t_{\mu}) = \Omega \mathbf{F} \bar{\mathbf{x}}(t_{\mu}), \quad (14)$$

recall (3,11,12). Define also the (scaled) deviation of the data from this value,

$$\Delta = \frac{\mathbf{Y} - \bar{\mathbf{Y}}}{\sqrt{\Omega}}. \quad (15)$$

As in (6), the scaling is such that elements of Δ are typically of order unity. In the specific case considered here, the functional CLT states that the log-likelihood obeys

$$\log \mathcal{L}(\boldsymbol{\theta}) \simeq -\frac{1}{2} [\Delta^T \mathbf{G}^{-1} \Delta + \ln \det(2\pi \mathbf{G}/\Omega)] \quad (16)$$

where the approximate equality is accurate as $\Omega \rightarrow \infty$, and \mathbf{G}^{-1} denotes the inverse of a square covariance matrix \mathbf{G} , whose form is dictated by the CLT of Sec. IID: see Appendix A, in particular (A8). Given a compartment model with parameters $\boldsymbol{\theta}$ and a filter matrix \mathbf{F} , computation of \mathbf{G} requires numerical solution of a (matrix-valued) ODE.

Compared to the likelihood (16), an alternative is to use a deterministic model for the disease [8, 9, 11, 15, 30], with all stochasticity coming from the surveillance (or data collection) process. In this case the likelihood can be computed by solving a vector-valued ODE similar to (5), or a corresponding discrete-time equation. That approach is computationally cheaper, but it neglects stochasticity in disease transmission. Alternatively, one might consider direct evaluation of the likelihood by MCMC on the stochastic model [19, 38]. This route has a very high computational cost compared with (16), although it is more accurate than the CLT description in situations where compartment populations are low. In this sense, the CLT result is a practical compromise.

IV. INFERENCE METHODOLOGY

This Section briefly describes the inference methodology, as implemented in PyRoss [10, 26].

A. Model estimation

The methodology has been implemented for a general class of compartment models as defined above, including progression and infection transitions. Specifically, if transition ξ involves progression from compartment α , one has

$$w_\xi(t, \boldsymbol{\theta}, \mathbf{n}) = \gamma_\xi(t, \boldsymbol{\theta}) n_\alpha \quad (17)$$

with arbitrary dependence of γ_ξ on the parameters $\boldsymbol{\theta}$ and the time t . For infection reactions, suppose that transition ξ involves a susceptible individual in cohort i being infected by an individual in some infectious class. Denote the population of susceptible individuals in cohort i by S_i and the population of individuals in cohort j of the

infectious class by $I_j^{(k)}$; here k is a label for the relevant infectious class. Then the generic infection rate is

$$w_\xi(t, \boldsymbol{\theta}, \mathbf{n}) = \sum_{j=1}^M K_\xi(t, \boldsymbol{\theta}) \frac{S_i I_j^{(k)}}{\Omega}, \quad (18)$$

where K_ξ has arbitrary dependence on the parameters $\boldsymbol{\theta}$ and the time t . The form of K depends on the rates of contacts between cohorts and on various epidemiological parameters, a specific example is given in Sec. V below.

Once the model is specified, the inference methodology is automated. We outline the method, with details in Appendix B and [10]. Given the data and some parameter values $\boldsymbol{\theta}$, the (non-normalised) posterior is computed (up to the normalisation factor Z) by combining the prior information with (16). This posterior is optimized over $\boldsymbol{\theta}$ using the covariance maximisation evolutionary strategy (CMA-ES) [39], yielding the maximum a posteriori (MAP) parameters $\boldsymbol{\theta}^*$. We also compute the Hessian matrix of the log-posterior using finite differences.

We consider the Fisher information matrix (FIM) [16], which measures the information provided by the data about the inferred parameters of the model. It is a matrix with elements

$$\mathcal{I}_{ab}(\boldsymbol{\theta}) = -\left\langle \frac{\partial^2}{\partial \theta_a \partial \theta_b} \log \mathcal{L}(\boldsymbol{\theta}) \right\rangle, \quad (19)$$

where the angled brackets denote an average over the stochastic dynamics of the model, with fixed parameters $\boldsymbol{\theta}$. Recalling (13), this means that one averages over all possible values of \mathbf{Y} according to the model dynamics, instead of using the observed data. The sensitivity of parameter a with respect to the (expected) data can then be estimated as

$$s_a = \theta_a^* \sqrt{\mathcal{I}_{aa}(\boldsymbol{\theta}^*)}, \quad (20)$$

for more detail see [40, 41]. The FIM is defined as an average over the stochastic dynamics, but the Gaussian structure of the likelihood (16) means that the FIM can be estimated by a deterministic computation, see Appendix B 1.

To go beyond the MAP, we sample the posterior for $\boldsymbol{\theta}$ using MCMC, using the emcee package [42]. We compute the model evidence Z in (10) using thermodynamic integration, see Appendix B 2. The evidence is useful for Bayesian model comparison and model averaging [28], an example of model comparison is given in Sec VIC below. A given model has high evidence if it can fit the data accurately with parameters that are consistent with the prior and do not require fine-tuning. The fit to the data can be assessed separately via the posterior average of the log-likelihood $\mathbb{E}_{\text{post}}[\log \mathcal{L}]$, which helps to disentangle the contributions to the evidence.

B. Forecasts and nowcasts

Given samples from the posterior, several kinds of forecast and nowcast are possible. The time period over

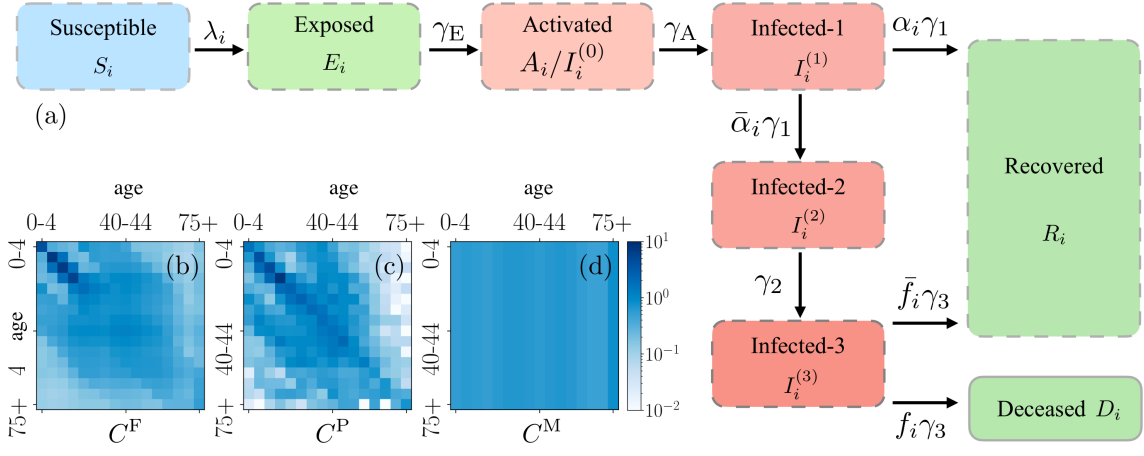


FIG. 1: (a) Epidemiological classes of the example model, with rate constants indicated (the infection rate λ_i is defined in Appendix C 1). Here $\bar{\alpha}_i = 1 - \alpha_i$ and similarly $\bar{f}_i = 1 - f_i$. The coloring distinguishes susceptible, infectious, and non-infectious compartments. The transition $I^{(1)} \rightarrow R$ represents rapid recovery of asymptomatic/paucisymptomatic cases, see main text. (b,c,d) Contact matrices for the different model variants.

which data is used for inference is called the *inference window*.

In a *deterministic* forecast or nowcast, we compute the average path $\bar{\mathbf{x}}(t)$ for a given set of parameters. This allows prediction of the population of unobserved (latent) compartments. If this is performed for times t within the inference window, we refer to it as a nowcast. The path $\bar{\mathbf{x}}(t)$ can also be computed outside this window, this is a forecast. By sampling parameters from the posterior, the range of behaviour can be computed. However, this computation only captures the role of parameter uncertainty, it neglects the inherent stochasticity of the model.

In a *conditional* nowcast, we use the functional CLT to derive a (Gaussian) distribution for the population of the latent compartments, conditional on the observed data. Samples from this distribution can be generated, which allow the role of stochasticity to be assessed, see Appendix B 3. We emphasise that the nowcast requires sample paths that are conditional on the data, for times within the inference window. Such conditional distributions cannot be sampled by direct simulation of the model, but the functional CLT enables sampling (under the assumption of large Ω).

Finally, we consider stochastic trajectories that extend beyond the inference window, which we call a *stochastic* forecast. In this case we first use a conditional nowcast to sample the latent compartments at the end of the inference window, after which we simulate the stochastic dynamics (by Gillespie [43] or tau-leaping methods [44]). This yields trajectories of the full stochastic model, with integer-valued populations. (Contrary to the conditional nowcast, these sample paths are only conditional on data from the past. Hence they can be sampled directly, due to the Markov property.)

V. COVID-19 IN ENGLAND AND WALES : MODEL

To illustrate these methods, we analyse a well-mixed compartment model for England and Wales, using data published by the Office for National Statistics (ONS), for numbers of deaths where COVID-19 was mentioned on the death certificate [45]. We consider the period 6-March to 15-May 2020, which covers the imposition of lockdown, and the associated peak in weekly deaths. (The first recorded deaths took place in the week ending 6-March, the lockdown was imposed on 23-March, and the peak in deaths was in late March and early April.) In numerical data, time is measured in weeks, starting from 6-March.

The model uses time-dependent contact structures to model for a non-pharmaceutical interventions (NPIs), which includes the lockdown as well as other behavioural changes (mask wearing, additional hand washing, etc). For consistency with the well-mixed assumption of the model, our data excludes deaths taking place in care homes, since these individuals likely have unusual contacts, which are primarily inside their own institutions.

More precisely, individuals in the model are defined to exclude care-home residents, and we assume negligible transmission of infection from care homes to non-residents. (Note, there is no such assumption on transmission in the opposite direction, from non-residents into care homes.) We also assume (i) that all deaths in care homes were for individuals aged 75+, and (ii) that the care-home population is small in comparison to the total, so that the N_i are fixed at the total cohort populations, without being adjusted to exclude care-home residents. These assumptions simplify the model; they are not perfectly accurate, but we argue that the associated approximations are negligible compared with the (coarse) well-mixed assumption discussed in Sec. II B, and the un-

certainties in the identification of COVID-related deaths.

A. Definition and epidemiological parameters

We consider $M = 16$ age cohorts, which correspond to 5-year age bands from 0-4 to 70-74, and a single cohort for all individuals of age 75+. The population of cohort i is N_i and $\Omega = \sum_i N_i$. Given the short time period considered here, we neglect vital dynamics (birth, aging and death by causes other than COVID-19).

There are $L = 8$ epidemiological classes, illustrated in Fig. 1. Susceptible individuals (S) move to the exposed class E when they become infected. The exposed class represents the latent period so these individuals are not infectious; they progress with rate γ_E to an activated class A , which is infectious but non-symptomatic. We sometimes also denote this class by $I^{(0)}$. From A , all individuals progress to class $I^{(1)}$, with rate γ_A . Hence $I^{(1)}$ includes cases that never develop symptoms, as well as paucisymptomatic and severe cases. (Paucisymptomatic cases are defined as those with very mild symptoms, following [46].) These situations are distinguished by their progression from stage $I^{(1)}$ – the total progression rate is γ_1 , with an age-dependent fraction α_i of individuals (asymptomatic/paucisymptomatic cases) recovering into class R ; the remainder progress to a symptomatic infectious stage $I^{(2)}$. There is progression from $I^{(2)}$ to $I^{(3)}$ with rate γ_2 . After this, the (total) progression rate from $I^{(3)}$ is γ_3 , of which an age-dependent fraction f_i of individuals die (transition to D) while the remainder recover to R . Hence f_i corresponds to the case fatality ratio (CFR), and the infection fatality ratio is $(1 - \alpha_i)f_i$.

Individuals in R are immune, we assume no reinfection within the period considered in this work. The inclusion of several infectious stages allows flexibility in the model as to the distribution of times between infection and recovery or death.

The infection process for cohort i depends on a contact rate matrix \tilde{C} , the susceptibility to infection of that cohort β_i , and on how infectious is the infected individual. The rate for infection of individuals in cohort i by those in infectious stage k is

$$w_\xi(t, \boldsymbol{\theta}, \mathbf{n}) = \beta_i S_i \sum_{j=1}^M \tilde{C}_{ij}(t) \frac{\nu_k I_j^{(k)}}{N_j} \quad (21)$$

where S_i is the population of the relevant susceptible compartment, also $I_j^{(k)}(t)$ is the population of the infectious stage for cohort j , and ν_k is the infectiousness of stage k . There are separate transitions ξ for infection of every cohort i , and for every infectious stage k . Comparing (18,21) shows that $K_\xi(t, \boldsymbol{\theta}) = \beta_i \tilde{C}_{ij}(t) \nu_k \Omega / N_j$ for this transition. The choice of contact (rate) matrix is discussed in Sec. VB, below. The (deterministic) equations that describe the average evolution of this model are given in Appendix C 1.

Since we only consider data for numbers of deaths, it is not possible to infer all epidemiological parameters. For example, the data do not provide information about absolute numbers of cases, nor on the relative numbers of symptomatic and asymptomatic cases. For this reason, we fix the α and f parameters to estimated (age-dependent) values based on [46]. These estimates are discussed in Appendix C 2, they are subject to considerable uncertainty, but the resulting model is still flexible enough to fit the data. All remaining parameters are inferred. The β parameters are age-dependent, all other epidemiological parameters are assumed independent of age. As noted above, the initial condition $\mathbf{x}(0)$ must be determined from the inference parameters $\boldsymbol{\theta}$. Details of this procedure, and full specification of all prior distributions are given in Appendix C 2.

B. Model variants (contact matrices and NPIs)

We consider a Bayesian model comparison, based on several variants of the model described above, which differ in their contact structure.

In the absence of any NPI, infective contacts are described by (bare) contact matrices \mathbf{C} , such that C_{ij} is the mean number of contacts per day with individuals in cohort j , for an individual in cohort i . To account for NPIs we assume that individuals in cohort i have their activities multiplied by a time-dependent factor $a_i(t) \leq 1$, so that the mean number of contacts per day during the NPI is changed to $a_i(t)C_{ij}a_j(t)$. In the absence of any intervention then $a_i = 1$. Note also, C_{ij} is a number of contacts, but the quantity \tilde{C}_{ij} that appears in (21) is a contact rate; hence we take

$$\tilde{C}_{ij} = \eta a_i(t) C_{ij} a_j(t) \quad (22)$$

where η is a basic rate of 1 (day)⁻¹. Our numerical implementation measures time in weeks, so $\eta = 7$ (week)⁻¹.

We consider three possibilities for the bare contact matrix \mathbf{C} , see Fig. 1 and Appendix C 3. Two of the choices are the matrices proposed by Prem et al [48] and Fumanelli et al [49], which are both based on the POLYMOD study [50]. The third is a simple proportional mixing assumption, which is that individuals meet each other at random:

$$C_{ij} = c_0 \frac{N_j}{\Omega} \quad (23)$$

where c_0 is a constant chosen to have a total number of contacts comparable to that of [48]. We refer to the resulting contact matrices (and the associated model variants) as C^F, C^P, C^M for the models of Fumanelli et al [49], Prem et al [48], and proportional Mixing, respectively. We do not distinguish at all between different types of contact (for example home, work, school), the reasons for this are discussed in Sec. VIA, below.

We also consider two possibilities for the NPI parameters $a_i(t)$, as shown in Fig. 2. These were chosen to

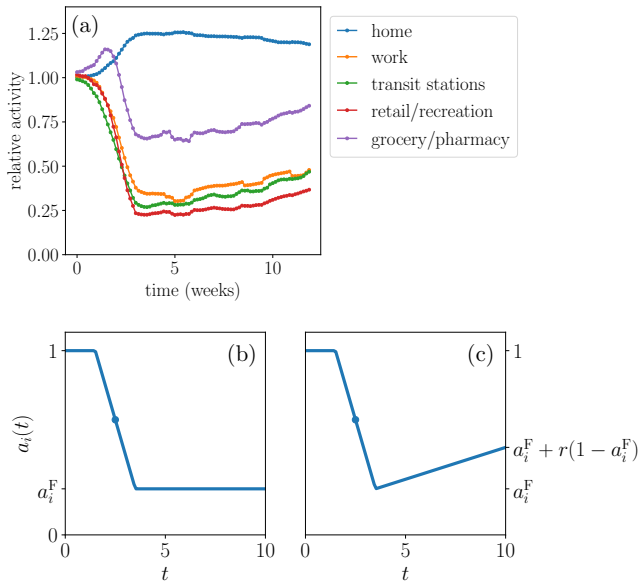


FIG. 2: (a) Data for time spent in different activities, published by Google (UK data) [47], smoothed with a 7-day rolling average. (b) Time-dependence of step-like-NPI, (c) NPI-with-easing, the easing factor is r .

mimic the patterns of activity in the UK, based on data published by Google [47]. The first possibility is a step-like-NPI, with a linear decrease from $a_i = 1$ to $a_i(t) = a_i^F$ over a time period W_{lock} , after which $a_i(t)$ remains constant at a_i^F . The mid-point of the step-like decrease is at time t_{lock} , the parameters of the NPI are t_{lock} , W_{lock} and the various a_i^F . The second possibility is an NPI-with-easing, it involves the same step-like decrease, followed by a linear increase, such that the value at the end of the period considered is $a_i^F + r(1 - a_i^F)$, where r is an additional lockdown-easing parameter (larger values correspond to more contacts). Priors and further details are given in Appendix C 2.

VI. COVID-19 IN ENGLAND AND WALES: RESULTS

We have applied the methodology of Sec. IV to the models of Sec. V. The total number of inference parameters (for initial conditions, epidemiological parameters, and contact structure) is either 46 or 47, depending on the NPI. This number could be reduced by considering a smaller number of age cohorts, but we retain them here to illustrate that the methodology is applicable in models of this complexity.

As a baseline, we perform inference using data for the 7-week period 6-March 2020 to 24-April 2020, with the remaining 3 weeks of our data period used to assess the resulting Bayesian forecast.

A. Step-like NPI

Fig. 3(a,b) show results for the C^F model variant with step-like NPI, and 7 weeks used for inference. We show the cumulative number of deaths by cohort, for the deterministic trajectory $\bar{x}(t)$, obtained using the MAP parameter values. The model matches well the data. Note the model results are averages so the cohort populations are not integer-valued in general. Small populations (and particularly those below 1) indicate that the assumptions of the CLT are questionable, but in practice the likelihood is dominated by compartments with large populations, in which case (16) is still a reasonable approximation. (The data have no deaths in the 5-9 cohort, for this time period.)

Fig. 3(c) shows deterministic forecasts with step-like NPIs (recall Sec. IV B), based on the different contact matrices. Parameters are sampled from the posterior (as obtained by MCMC). The model variants behave almost identically and fit the data used for inference. However, the forecasts are not accurate. We attribute this primarily to lockdown easing – this is neglected within the model shown (which has $r = 0$), so an accurate forecast should not be expected. Forecasting is explored further in Sec. VI C, including more realistic models with $r > 0$.

Fig. 4(a) shows inferred values of latent (unobserved) compartments, using a deterministic nowcast with parameters from the posterior. As expected, they show a rise and fall in the number of infected individuals, with different stages having their peaks at different times. An important set of (age-dependent) parameters are the β_i , which determine the susceptibility to infection. Fig. 4(b) shows inferred values of β_i for the C^F model, including the range of posterior samples, and the posterior mean, which are compared with the MAP estimate and the prior. The inferred values of β are quite far from the prior mean; these parameters are very uncertain a priori. (This uncertainty is incorporated by using log-normal priors for the β_i with a standard deviation one half of the mean, see Appendix C 2.) The main feature in the inferred result is the large value of β_i for the oldest cohort (75+). The inferred values of other parameters are discussed in Appendix C 4, they are generally consistent with the prior assumptions.

To rationalize the inferred β , it is easily verified that for a model with the assumed contact structure, CFR and α , the inferred value of β for the oldest cohort must be larger than all other cohorts, in order to capture the age-dependence of deaths in England and Wales, which are very skewed towards the older age groups. There are at least two reasons why inference might lead to such a large β : either the assumed CFR (or α) has too weak an age-dependence which is being compensated by an age-dependent β ; or the contacts of elderly individuals are indeed more likely to result in infection, perhaps for medical reasons, or because of increased time in high-risk environments (such as hospitals). This distinction could be settled if accurate data for numbers of infec-

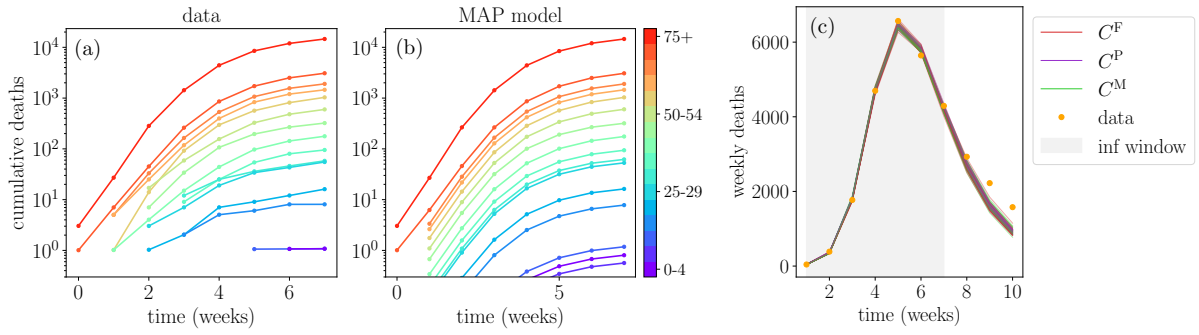


FIG. 3: (a,b) Comparison of data with MAP trajectory for cumulative deaths (C^F model variant with step-like-NPI). (c) Deterministic forecast for step-like-NPI with various model variants. There are 20 trajectories for each model variant, with parameters sampled from the posterior.

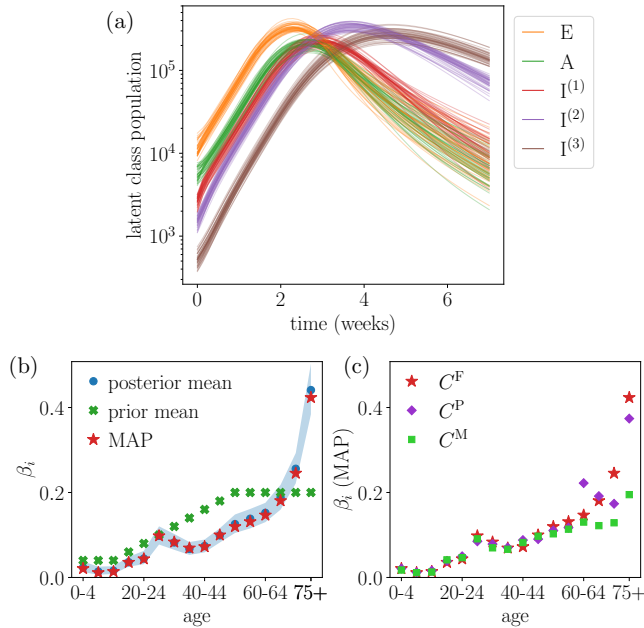


FIG. 4: Results with step-like-NPI (a) populations of latent compartments (summed over age cohorts), 40 deterministic trajectories, corresponding to parameter samples from the posterior. (b) Inferred (posterior) β_i from MCMC (using C^F variant), shading shows 5th to 95th percentiles. The MAP and prior mean are also indicated. (c) Inferred (MAP) β_i for different model variants.

tions were included in the analysis, but it is not possible with the data considered here. The results of [9] suggest that susceptibility is age-dependent, but the dependence is weaker than we infer, indicating that both effects are in play.

Fig. 4(c) shows the (MAP) inferred β parameters for the models with different contact matrices. While the trend is similar, there are significant differences. Nevertheless, the behaviour of the inferred models is almost identical, recall Fig. 3(c). The reason is that the behaviour of the model is dominated by the infection rates

of (21) – different contact matrices can still lead to similar model behaviour, because of the freedom to adjust the β_i . In this sense, our results can be interpreted as inference of an “infective contact matrix” whose elements are $\beta_i C_{ij}$. It is notable from Fig. 1 that the C^P contact matrix includes some large differences between cohorts with similar ages, particularly in contacts with the 75+ cohort. These can be traced back to the finite data set of the original POLYMOD study [50]. For the C^P model variant, these large fluctuations lead to an inferred β_i with a complicated dependence on age, for cohorts in the 60+ group. In the C^F variant, the dependence on age is much smoother, both for contacts and for β . Compared to the contact matrices that are based on POLYMOD [48, 49], the C^M variant has (much) more contacts for older individuals, so the inferred β is lower in the older cohorts.

B. Fisher information matrix and model evidence

We now discuss the FIM (19) for the C^F model variant with step-like-NPI. Two items of particular interest are parameters θ_a whose inferred values are very sensitive to the data, and soft modes of the parameter space along which the likelihood varies slowly. These modes indicate aspects of the model that are mostly determined by the prior.

The sensitivities of (20) provide useful information on the first point. Fig. 5 shows results. The parameters most sensitive to the data are the rates γ_E , γ_A and γ_1 , the probability of the oldest age cohort to get infected β_{75+} , and the time of lockdown t_{lock} , consistent with the discussion so far. These parameters have $s_a > 100$, indicating that changes of order 1% in their values are sufficient to change the log-likelihood by an amount of order unity.

Soft directions around the MAP parameters, in which the model behaviour is expected to change very little, do exist. They arise from small eigenvalues of the FIM, and the corresponding eigenvectors. One example of such a

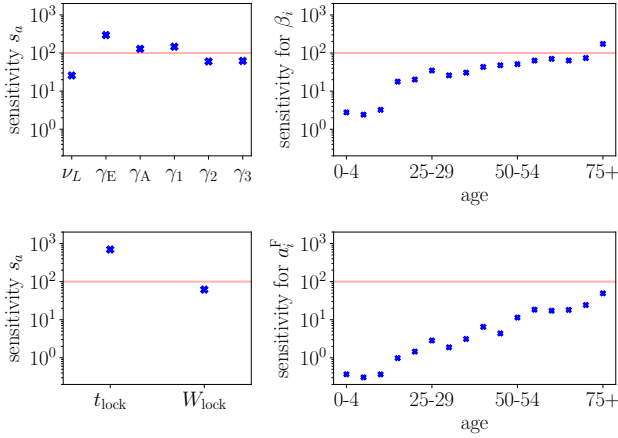


FIG. 5: Fisher information matrix: sensitivities for model parameters. Red lines show the value 100, as an (arbitrary) indication of parameters that are very sensitive to the data. Similar results for the parameters that determine the initial condition are given in Appendix C 4.

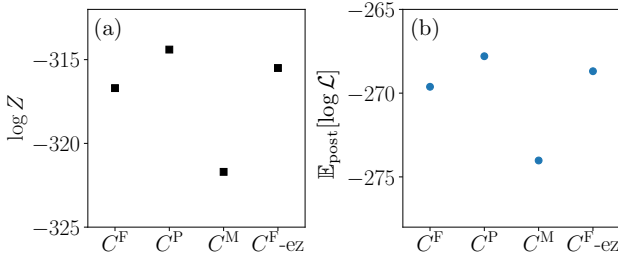


FIG. 6: (a) Model evidence for different model variants. The notation C^F -ez indicates the C^F model variant and NPI-with-easing; all other results are for step-like-NPI. (b) Posterior mean log-likelihood: this indicates the extent to which the inferred models fit the data.

soft mode is discussed in Appendix C 4. The existence of soft modes speaks in favour of a Bayesian approach, in that prior information about the disease is used to fix those parameters which are not determined by the data. This makes best use of all information sources, including expert-derived priors. (For experiments in the physical sciences, one might hope for enough data that the inferred parameters depend weakly on the prior, but that is not possible in this context.)

We have also computed the evidence for these models, see Fig. 6. The C^F and C^P contact matrices lead to similar log-evidences, with the C^P variant higher by around 3 units (we use natural logarithms throughout). The contact matrix with proportional mixing leads to log-evidence that is smaller by around 8 units. We conclude that this model can still fit the data with reasonable accuracy, but the inference computation is sensitive enough to infer that the contact structure has some assortativity. Also shown is the posterior mean of the log-likelihood $\mathbb{E}_{\text{post}}[\log \mathcal{L}]$, which has similar behaviour to the evidence.

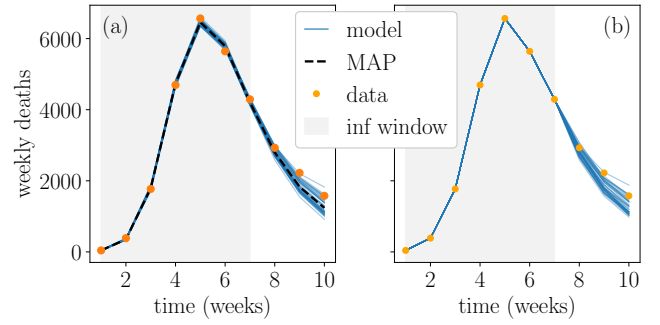


FIG. 7: Deterministic and stochastic forecasts, NPI-with-easing, C^F model variant. (a) deterministic (averaged) forecast, 40 trajectories with parameters from posterior; (b) stochastic forecast conditional on data. Compared with Fig. 3c, the effect of lockdown easing is to increase in deaths at later times, which improves the agreement with data.

This indicates that the differences come primarily from the quality of the fit.

Given the very naive assumptions of the proportional mixing model, we argue that the difference of 8 units in log-evidence should be regarded as a mild effect. Our conclusion is that the inference computation is not extremely sensitive to prior assumptions on the contact structure. Based on this result, it seems that more detailed modelling of contacts (for example separation by work/home/school) will have relatively little impact on the quality of inference, given the very large uncertainties within the model about the values of β_i .

C. NPI-with-easing

We now consider NPI-with easing. Since the behaviour with different contact matrices is very similar, we restrict to the C^F model variant.

Fig. 7(a) is a deterministic forecast analogous to Fig. 3(c); it shows how the easing parameter r leads to increased uncertainty in the forecast, in a way that is more consistent with the data. By contrast, Fig. 7(b) shows a stochastic forecast as defined in Sec. IV B. This accounts for stochasticity in the epidemiological dynamics, it automatically matches the data within the inference window. The results of the two kinds of forecast are similar, indicating that the dominant source of uncertainty is coming from the model parameters.

To explore the effects of lockdown easing in more detail, we consider the effect of increasing inference window, always comparing the model forecasts for the same 10-week period. Results are shown in Fig. 8. The agreement between inferred model and the data increases, as expected – we find that this model can accurately fit the data, with reasonable parameter values.

For the 7-week inference window, Fig. 9 shows that the distribution of r is still close to the prior. This is consistent with the result of Fig. 6, that the evidence

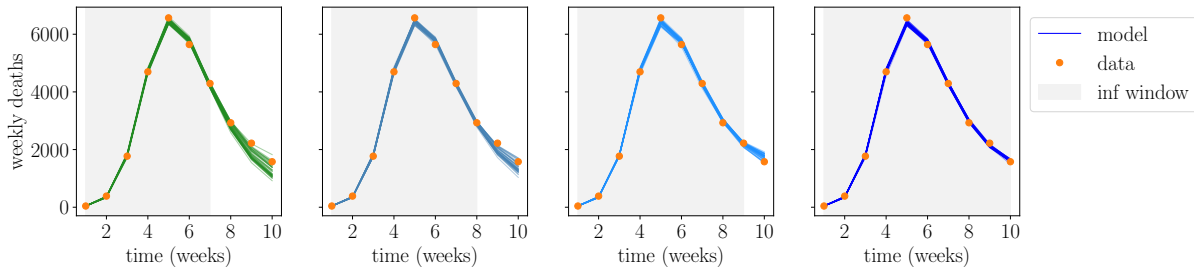


FIG. 8: Deterministic forecasts showing the effect of increasing the time period used for inference from 7 to 10 weeks. (C^F model variant, NPI-with-easing).

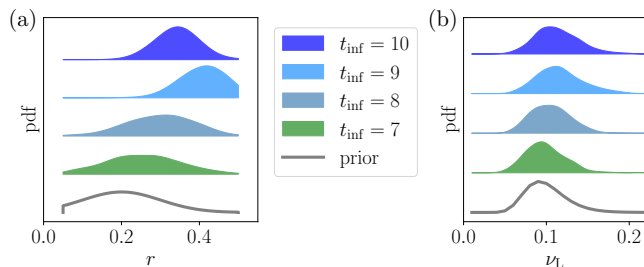


FIG. 9: Posterior distributions of the easing parameter r , and the late-stage infectiousness factor ν_L , as the inference time period t_{inf} is increased. (C^F model variant, pdfs are shown as Gaussian kernel density estimates.)

of the variant with easing is comparable to the variants with step-like-NPI. That is, the additional parameter r leads to a mild improvement in the fit to the data, and fine-tuning of its value is not required.

When considering longer time windows, we note that deaths are lagging indicator of the number of cases, which means that r is still not fully determined by the data. That is, these results still depend significantly on the prior (for details see Appendix C 2). Nevertheless, increasing the inference window causes the posterior distribution of r to shift towards larger values, leading to improved agreement with the data. There are also significant differences in these posterior distributions, for example if 9 or 10 weeks data are used for inference – this limits the robustness of the forecasting and indicates a possible tendency to over-fitting. We attribute this primarily to the simple linear easing assumed in our NPI. Most other parameters depend weakly on the period used for inference (see Appendix C 4).

In evaluating these results, we note that both the model and the likelihood assume a well-mixed population. In practice, individuals have correlated behaviour, which can be expected to enhance stochastic fluctuations. For this reason, it is likely that the functional CLT underestimates the variance of the data, given the model. This can lead to an over-fitting effect. There are also uncertainties in the data that are not accounted for in the likelihood, such as possible under-detection of COVID-related

deaths in the early period of the epidemic. Recalling that the deceased population in the model includes only those individuals who were diagnosed with COVID-19, such an under-detection might be modelled (in this framework) by a time-dependent CFR.

VII. DISCUSSION

We have described a methodology for inference and forecasting in epidemiological compartment models, where all stochastic aspects of disease propagation and measurement are modelled on an equal footing, and the likelihood is justified from first principles, and derived directly from the model. This means that the likelihood can be computed directly from the model definition, given appropriate data.

This methodology has been used to calibrate a model for the COVID-19 pandemic in England and Wales, based on death data. We have compared models with different contact structures, showing that fine details of the contact matrix have very little effect on model behaviour and forecasts. Indeed, the model with proportional mixing behaves very similarly to those with contact matrices derived from the POLYMOD data set [48–50]. This may be surprising at first glance, but the fact that the β_i parameters are inferred separately for each cohort means that the model has enough flexibility to infer how many infective contacts are made by each group. More specifically, it is the infection rate constant K of (18) that determines the model behaviour, so one sees from (21) differences in contact matrices can be partially compensated by changes in β . (The compensation is only partial because while β_i controls the relative numbers of infections, the contact matrix also determines the assortativity of mixing.)

In contrast to the details of mixing among cohorts, modelling assumptions about time-dependence of the contact structure have a significant impact on forecasting, as one should expect. This is illustrated by the dependence of the behaviour on the easing factor r .

Within the time period considered, the model gives forecasts that are reasonably accurate and robust. How-

ever, we have identified a possible tendency to over-fitting, some of which may be due to the well-mixing assumption that is used in the likelihood. Another common approach uses negative binomial distributions in the likelihood [8, 9, 15], this corresponds to a larger variance for numbers of deaths (over-dispersion), compared to the CLT. It would be interesting to consider inclusion of an over-dispersion factor in the likelihood used here, as a way of accounting for correlations in the contact structure.

In terms of model calibration, the main limitation of this study is the fact that we do not use data for case numbers, which means that the CFR cannot be inferred. In the UK, the rates and policies for testing for COVID-19 have had complex time-dependence, which means that robust estimation of case numbers is challenging. Incorporation of a time-dependent testing capacity into this framework is a direction of ongoing research. The extension of this framework to geographically-resolved models is also under active investigation.

Acknowledgments

We thank Graeme Ackland, Daniela de Angelis, Paul Birrell, Daan Frenkel, Sanmitra Ghosh, and Ken Rice for helpful discussions. We also thank PyRoss contributors, Fernando Caballero, Bilal Chughtai, Jules Guioth, and Benjamin Remez; and JPM researchers William Bankes, Erik Brorson, Andrew Ng, and William Peak. This work was undertaken as a contribution to the Rapid Assistance in Modelling the Pandemic (RAMP) initiative, coordinated by the Royal Society. This work was funded in part by the European Research Council under the Horizon 2020 Programme, ERC grant 740269, and by the Royal Society grant RP17002. The authors are also grateful for financial support from the EPSRC doctoral training programme (A.B., J.D., G.T.), the Leverhulme Trust (P.B.R. and H.K.), the Cambridge Trust and Jardine foundation (Y.I.L.).

Author contributions

The integration of epidemiological modelling, the Bayesian estimation of models against epidemiological data, and the optimisation of NPIs in these fitted models was conceived by R.A., who also led the PyRoss project, with additional guidance from M.E.C. Development of the model for England and Wales was led by R.L.J.. The inference methodology was developed by Y.I.L., G.T., P.B.R., and P.P., with specific contributions including functional CLT (Y.I.L.); Fisher information matrix (G.T.); evidence and MCMC (P.B.R.); and likelihood computation (P.P.). Also, J.K. developed stochastic simulation and forecasting; R.S. designed the numerical implementation of PyRoss and developed deterministic simulations; and J.D. developed the example model.

Contributions by T.E., L.K., A.B., and J.D.P. enabled flexible inference for compartment models, and H.K. contributed to the stochastic forecasts. The manuscript was written by R.L.J. and R.A., with contributions from all authors.

Appendix A: Derivation of \mathbf{G} for likelihood

This Appendix derives the covariance matrix \mathbf{G} that appears in the likelihood (16). The result is based on the CLT for \mathbf{u} discussed in Sec. IID. We first compute a covariance matrix $\tilde{\mathbf{G}}$ for the state \mathbf{u} , from which we derive the covariance \mathbf{G} of the data.

Note that \mathbf{J} and σ_ξ in (7) depend on the deterministic path $\bar{\mathbf{x}}$ but not on the random variable \mathbf{u} , so (7) is a time-dependent Ornstein-Uhlenbeck process. This enables derivation of three important results. The first concerns the covariance matrix Σ for $\mathbf{u}(t)$, whose elements are

$$\Sigma_{ij}(t) = \langle u_i(t)u_j(t) \rangle. \quad (\text{A1})$$

Here and throughout, angled brackets $\langle \cdot \rangle$ denote an average over the stochastic dynamics of the compartment model. [Recall that $\mathbf{u}(0) = 0$ so $\langle \mathbf{u}(t) \rangle = 0$ and also $\Sigma_{ij}(0) = 0$.] The equation of motion for Σ can be derived from (7) as

$$\begin{aligned} \frac{\partial}{\partial t} \Sigma(t) = & \mathbf{J}(t, \boldsymbol{\theta}, \bar{\mathbf{x}}_t) \Sigma(t) + \Sigma(t) \mathbf{J}^T(t, \boldsymbol{\theta}, \bar{\mathbf{x}}_t) \\ & + \mathbf{B}(t, \boldsymbol{\theta}, \bar{\mathbf{x}}_t) \end{aligned} \quad (\text{A2})$$

where

$$\mathbf{B}(t, \boldsymbol{\theta}, \bar{\mathbf{x}}_t) = \sum_{\xi} \sigma_{\xi}(t, \boldsymbol{\theta}, \bar{\mathbf{x}}_t) \sigma_{\xi}^T(t, \boldsymbol{\theta}, \bar{\mathbf{x}}_t) \quad (\text{A3})$$

is a square matrix. Equ. (A2) can be solved (numerically) for Σ .

Second, let $\langle \cdot \rangle_{\mathbf{u}(s)}$ denote an average, conditional on the value of $\mathbf{u}(s)$. Taking the first moment of (7) one arrives at a linear equation for the average value of \mathbf{u} , hence for $t \geq s$ one has

$$\langle u_i(t) \rangle_{\mathbf{u}(s)} = \sum_j U_{ij}(s, t) u_j(s) \quad (\text{A4})$$

where the matrix $\mathbf{U}(s, t)$ is the time-evolution operator, which solves the linear differential equation

$$\frac{\partial}{\partial t} U_{ij}(s, t) = \sum_k J_{ik}(t, \boldsymbol{\theta}, \bar{\mathbf{x}}_t) U_{kj}(s, t) \quad (\text{A5})$$

with initial condition $U_{ij}(s, s) = \delta_{ij}$. This equation is readily solved (numerically) for \mathbf{U} .

The third result can then be obtained by noting that the covariance matrix for \mathbf{u} between two times s, t can be

obtained (for $t \geq s$) by composing the covariance $\Sigma(s)$ with the propagator $U(s, t)$. That is,

$$\langle u_j(s)u_i(t) \rangle = \sum_k \Sigma_{jk}(s)U_{ik}(s, t). \quad (\text{A6})$$

To exploit this last result, consider the vector obtained by concatenating the full state of the system over observed time points, analogous to (12)

$$\mathbf{X} = (\mathbf{x}(t_1), \mathbf{x}(t_2), \dots). \quad (\text{A7})$$

Its mean is clearly $\bar{\mathbf{X}} = (\bar{\mathbf{x}}(t_1), \bar{\mathbf{x}}(t_2), \dots)$. Now define a (scaled) deviation from the mean as $\tilde{\mathbf{\Delta}} = (\mathbf{X} - \bar{\mathbf{X}})\sqrt{\Omega}$, and denote the covariance of this vector by $\tilde{\mathbf{G}}$. From (A6), this symmetric matrix is formed of blocks that depend on Σ and U :

$$\tilde{\mathbf{G}} = \begin{pmatrix} \Sigma(t_1) & \Sigma(t_1)U^T(t_1, t_2) & \dots \\ U(t_1, t_2)\Sigma(t_1) & \Sigma(t_2) & \dots \\ U(t_1, t_3)\Sigma(t_1) & U(t_2, t_3)\Sigma(t_2) & \dots \\ \vdots & \ddots & \ddots \end{pmatrix}. \quad (\text{A8})$$

Since (7) is an Ornstein-Uhlenbeck process, it can be shown additionally [34–36] that the distribution of $\tilde{\mathbf{\Delta}}$ is asymptotically Gaussian, with the given covariance $\tilde{\mathbf{G}}$. Since the observed data are related linearly to \mathbf{X} according to (11,12), one then obtains (16), with the covariance of $\mathbf{\Delta}$ given by

$$\mathbf{G} = \mathbf{F}\tilde{\mathbf{G}}\mathbf{F}^T. \quad (\text{A9})$$

Since all elements of $\tilde{\mathbf{G}}$ can be evaluated, this allows computation of the likelihood (16).

Appendix B: Implementation details for inference

1. Fisher information matrix

For a multivariate normal distribution, such as the likelihood obtained in Section III, with the mean vector $\bar{\mathbf{Y}}(\boldsymbol{\theta})$ and the covariance matrix $\mathbf{G}(\boldsymbol{\theta})$ the elements of the FIM (19) are [51]

$$\mathcal{I}_{a,b} = \frac{\partial \bar{\mathbf{Y}}^T}{\partial \theta_a} \mathbf{G}^{-1} \frac{\partial \bar{\mathbf{Y}}}{\partial \theta_b} + \frac{1}{2} \text{tr} \left(\mathbf{G}^{-1} \frac{\partial \mathbf{G}}{\partial \theta_a} \mathbf{G}^{-1} \frac{\partial \mathbf{G}}{\partial \theta_b} \right). \quad (\text{B1})$$

This form is advantageous since its computation only requires first order derivatives, which are estimated as finite differences.

2. Evidence computation

We use a thermodynamic integration method [52, 53] to compute the log-evidence

$$\log Z = \log \int_{\mathcal{D}} e^{\mathcal{A}(\boldsymbol{\theta})} P(\boldsymbol{\theta}) d\boldsymbol{\theta}, \quad (\text{B2})$$

where $\mathcal{A}(\boldsymbol{\theta}) = \log \mathcal{L}(\boldsymbol{\theta})$ is the log-likelihood, and the domain \mathcal{D} is the support of the prior $P(\boldsymbol{\theta})$. Compared to alternatives (for example nested sampling [54]), thermodynamic integration allows robust estimation of convergence, and its numerical uncertainties.

We summarise the method, which is based on an integration path from a tractable (and normalised) distribution

$$\tilde{P}(\boldsymbol{\theta}) = e^{\tilde{\mathcal{A}}(\boldsymbol{\theta})} P(\boldsymbol{\theta}) \quad (\text{B3})$$

to the posterior. To this end, define

$$f(z) = \log \int_{\mathcal{D}} e^{z[\mathcal{A}(\boldsymbol{\theta}) - \tilde{\mathcal{A}}(\boldsymbol{\theta})]} \tilde{P}(\boldsymbol{\theta}) d\boldsymbol{\theta}. \quad (\text{B4})$$

so that $f(0) = 0$ and $f(1) = \log Z$. Differentiating yields

$$f'(z) = e^{-f(z)} \int_{\mathcal{D}} [\mathcal{A}(\boldsymbol{\theta}) - \tilde{\mathcal{A}}(\boldsymbol{\theta})] e^{z[\mathcal{A}(\boldsymbol{\theta}) - \tilde{\mathcal{A}}(\boldsymbol{\theta})]} \tilde{P}(\boldsymbol{\theta}) d\boldsymbol{\theta}. \quad (\text{B5})$$

The right hand side is an expectation value $\mathbb{E}_{\pi_z}[\mathcal{A} - \tilde{\mathcal{A}}]$ with respect to the (normalised) intermediate distribution $\pi_z(\boldsymbol{\theta}) = e^{-f(z) + z[\mathcal{A}(\boldsymbol{\theta}) - \tilde{\mathcal{A}}(\boldsymbol{\theta})]} \tilde{P}(\boldsymbol{\theta})$. Given some $\tilde{\mathcal{A}}$, this expectation value can be estimated by MCMC. (Our choice for $\tilde{\mathcal{A}}$ is discussed just below.) Then the log-evidence can be expressed as

$$\log Z = \int_0^1 f'(z) dz. \quad (\text{B6})$$

To estimate this integral, we take a sequence $0 = z_0 < z_1 < \dots < z_n = 1$ and we use trapezoidal quadrature:

$$\log Z \approx \sum_{i=1}^n (z_i - z_{i-1}) \frac{f'(z_i) + f'(z_{i-1})}{2}. \quad (\text{B7})$$

For each quadrature point, $f'(z_i)$ is estimated by an MCMC computation of the expectation value (B5). These are independent MCMC estimates, which facilitates analysis of numerical uncertainties.

To select a suitable $\tilde{\mathcal{A}}$, the idea is that the closer is \tilde{P} to the posterior, the shorter is the integration path, and the easier the computation. However, \tilde{P} must be a normalised distribution on \mathcal{D} . A suitable choice for \tilde{P} is therefore a truncated Gaussian approximation to the posterior, around the MAP parameters $\boldsymbol{\theta}^*$. Let \mathbf{H} be the Hessian matrix of the (negative) log-posterior, whose elements are

$$H_{ab} = -\frac{\partial^2}{\partial \theta_a \partial \theta_b} [\log \mathcal{L}(\boldsymbol{\theta}^*) + \log P(\boldsymbol{\theta}^*)]. \quad (\text{B8})$$

Then the truncated Gaussian approximation of the posterior distribution is

$$\tilde{P}(\boldsymbol{\theta}|\mathbf{Y}) \propto \exp \left(-\frac{1}{2} (\boldsymbol{\theta} - \boldsymbol{\theta}^*)^T \mathbf{H} (\boldsymbol{\theta} - \boldsymbol{\theta}^*) \right). \quad (\text{B9})$$

for $\boldsymbol{\theta} \in \mathcal{D}$, and $\tilde{P} = 0$ otherwise. Rejection sampling is used to sample this distribution and to simultaneously obtain its normalisation constant, so that $\tilde{\mathcal{A}}(\boldsymbol{\theta}) = \log \frac{\tilde{P}(\boldsymbol{\theta}|\mathbf{Y})}{P(\boldsymbol{\theta})}$ can be computed, consistent with (B3). Hence (B7) can be computed.

3. Conditional nowcast

To sample latent compartments during the inference period, we use the CLT for \mathbf{u} discussed in Sec. IID. It is convenient to assume that the latent populations are to be inferred at the times t_μ where data was collected. (This assumption is easily relaxed, at the expense of some heavier notation.) Hence, the populations of the latent compartments are encoded in the vector \mathbf{X} of (A7). Given the model parameters, the distribution of \mathbf{X} obeys a CLT

$$\log P(\mathbf{X}|\boldsymbol{\theta}) \simeq -\frac{1}{2} \left[\boldsymbol{\Delta}^T \tilde{\mathbf{G}}^{-1} \boldsymbol{\Delta} + \ln \det(2\pi \tilde{\mathbf{G}}) \right], \quad (\text{B10})$$

analogous to (16), with $\tilde{\mathbf{G}}$ as in (A8). Since this distribution is (multivariate) Gaussian, and the data depend linearly on \mathbf{X} , it is straightforward to condition on the data and obtain a Gaussian distribution for the latent compartments, which can then be sampled.

Appendix C: Details and additional results for the example model

1. ODEs for average dynamics

For the (stochastic) model defined in Sec V, the deterministic equations for the mean (5) can be written in terms of the compartment populations. For this section alone, let S_i be the *average* population of susceptible individuals in cohort i , and similarly for all other classes. Our notation omits the dependence of these populations on time, for compactness. Using dots to indicate time derivatives, (5) becomes

$$\begin{aligned} \dot{S}_i &= -\lambda_i(t) S_i \\ \dot{E}_i &= -\gamma_E E_i + \lambda_i(t) S_i \\ \dot{A}_i &= -\gamma_A A_i + \gamma_E E_i \\ \dot{I}_i^{(1)} &= -\gamma_1 I_i^{(1)} + \gamma_A A_i \\ \dot{I}_i^{(2)} &= -\gamma_2 I_i^{(2)} + \bar{\alpha}_i \gamma_1 I_i^{(1)} \\ \dot{I}_i^{(3)} &= -\gamma_3 I_i^{(3)} + \gamma_2 I_i^{(2)} \\ \dot{R}_i &= \alpha_i \gamma_1 I_i^{(1)} + \bar{f}_i \gamma_3 I_i^{(3)} \\ \dot{D}_i &= f_i \gamma_3 I_i^{(3)}, \end{aligned} \quad (\text{C1})$$

where we do not indicate the dependence of the compartment populations on time (for compactness of notation), while $\bar{\alpha}_i = 1 - \alpha_i$ and $\bar{f}_i = 1 - f_i$, also

$$\lambda_i(t) = \sum_j \beta_i \tilde{C}_{ij}(t) \sum_{k=0}^3 \frac{\nu_k I_j^{(k)}}{N_j}. \quad (\text{C2})$$

Recall that $I_i^{(0)}$ should be identified as A_i and N_j is the total population of cohort j .

	distribution	mean	std/mean	bounds/mean
γ_E	Normal	(3.00 days) ⁻¹	0.1	(0.6,1.4)
γ_A	Normal	(2.50 days) ⁻¹	0.1	(0.6,1.4)
γ_1	Normal	(3.00 days) ⁻¹	0.1	(0.6,1.4)
γ_2	Normal	(7.25 days) ⁻¹	0.1	(0.6,1.4)
γ_3	Normal	(7.25 days) ⁻¹	0.1	(0.6,1.4)
β_i	Log-normal	(see caption)	0.5	(0.1,10)
ν_L	Log-normal	0.1	0.5	(0.1,10)
t_{lock}	Normal	17 days	0.06	(0.06,1.8)
W_{lock}	Normal	12 days	0.08	(0.008,1.7)
a_i^F	Log-normal	0.2	0.5	(0.01,10)
r	Normal	0.2	0.1	(0.05,0.5)

TABLE I: Priors for the compartment model, all parameters are independent with normal or log-normal distributions, as shown. The standard deviation (std) and bounds are quoted relative to the prior mean. The prior mean for β depends on the age cohort: $\beta_i = 0.2$ for ages 50+ and $\beta_i = 0.04$ for ages less than 15, with linear interpolation in the intermediate range. This age-dependence is based on [9], the overall scale was chosen so that the prior mean model is broadly consistent with exponential growth of cases in the first few weeks of the epidemic.

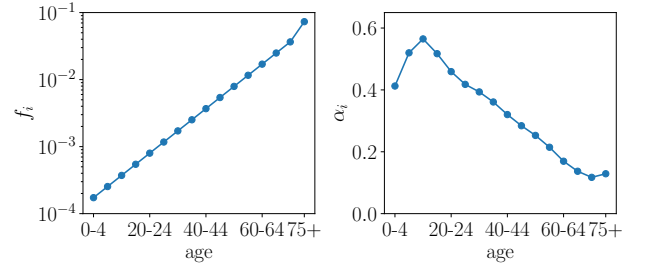


FIG. 10: Age-dependent parameters for the CFR f_i and the fraction of asymptomatic/paucisymptomatic cases α_i .

2. Parameters, priors and initial conditions

This section gives additional details of parameters in the model of Sec. V, and the priors used for inference. The infectiousness parameters ν_k are defined relative to the first infectious stage, so $\nu_1 = 1$. (This does not lose any generality because the ν parameters only appear through the combination $\beta_i \nu_k$.) In practice we parameterise ν in terms of a single inference parameter ν_L : we take $\nu_0 = \nu_1 = 1$, with $\nu_2 = \nu_3 = \nu_L$. The early stages of a COVID-19 case are much more infectious than later stages so $\nu_L < 1$, see below. The γ and ν parameters are assumed independent of age, while β, α, f, a are age-dependent.

The fixed (age-dependent) CFR was estimated from the data for 18-24 March in Table 4 of [46], by fitting an exponential dependence for ages 40-90 and then extrapolating this function to younger age groups. This leads to $f = A e^{(\text{age})/\xi}$ with $A = 1.43 \times 10^{-4}$ and $\xi = 13.1$ years. The fraction of asymptomatic/paucisymptomatic cases is

taken from Table 2 of [46], using linear interpolation to obtain values for the cohorts considered here. The relevant numbers are shown in Fig. 10. As discussed in the main text, these numbers are subject to considerable uncertainty, but the resulting model is flexible enough to fit the data used here. It would be valuable to incorporate additional data, to constrain these variables, for example through testing data, which can provide information on the number of cases.

The priors for inferred epidemiological parameters are summarised in Table I. The γ parameters are fixed by the disease itself and can be constrained based on medical data, see for example [55] for a discussion. We take Gaussian priors for these parameters with standard deviation 10% of the mean. Other parameters like β_i, ν_L, a_i, r are associated with disease transmission, and are much less well characterised, hence the use of less informative priors, which are log-normal with standard deviation 50% of the mean. (For positive parameters with large uncertainty, the log-normal prior is much more heavy-tailed than a Gaussian with the same standard deviation, while still penalising very small values.) The lockdown parameters t_{lock} and W_{lock} have a prior standard deviation of 1 day.

As noted in the main text, the initial condition $\mathbf{x}(0)$ is determined from the parameters θ . A simple estimate is available by linearising the average dynamics (5) about the state \mathbf{x}_S where all individuals are susceptible. The behavior of the resulting equation (at early times) is dominated by the largest eigenvalue of the matrix $\mathbf{J}(0, \theta, \mathbf{x}_S)$, as obtained from (8). The corresponding eigenvector dominates the evolution of the early stages of the epidemic, up to transient effects of the initial condition, which are controlled by the smaller (sub-dominant) eigenvalues. A suitable baseline estimate for the initial condition is then

$$\mathbf{x}_{\text{lin}}(0) = \mathbf{x}_S + \kappa \mathbf{v}_\theta^* \quad (\text{C3})$$

where \mathbf{v}_θ^* is the dominant eigenvector (which depends on the epidemiological parameters), and κ is an inference parameter. The normalisation of the eigenvector is $\sum_\alpha |v_{\theta,\alpha}^*| = 1$ where $v_{\theta,\alpha}^*$ is the α -th element of the vector \mathbf{v}_θ^* ; this means that the value of κ is approximately one half of the non-susceptible (infected + recovered + deceased) fraction of the population, at $t = 0$.

In practice our initial condition is obtained by modifying $\mathbf{x}_{\text{lin}}(0)$. First, the D (deceased) compartments are initialised from the observation data, which overrides the value from the dominant eigenvector. Second, the $E, A, I^{(k)}$ compartments for the oldest cohort are determined by a separate procedure (detailed in the next paragraph), which allows extra flexibility in the inference. Finally, the S compartments (for all age cohorts) are chosen to enforce the (fixed) total population of each cohort. [Using (C3) automatically ensures the correct cohort populations, but modifying $\mathbf{x}(0)$ from $\mathbf{x}_{\text{lin}}(0)$ means that compensation is required, to enforce this constraint.]

The modified initial condition for the oldest cohort is

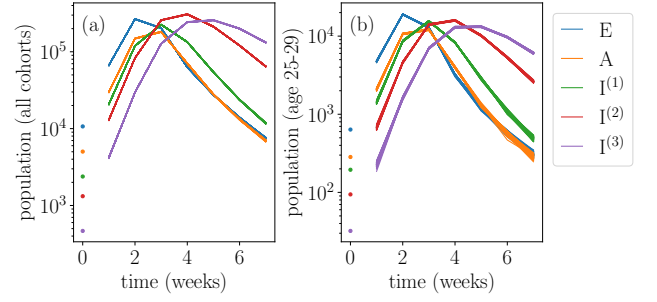


FIG. 11: Sampling of latent variables conditional on the data, to illustrate the size of the fluctuations described by the functional CLT. (a) Total population in each epidemiological class, as obtained from a conditional nowcast with 100 trajectories, using with MAP parameters. The dots indicate the inferred (MAP) initial condition. (C^F model variant with step-like-NPI). (b) Population of latent compartments for a single cohort (age 25-29), the stochastic fluctuations more apparent at this level.

based on a hypothesis that infections started in younger age groups, before spreading into the elderly population. The inferred result is consistent with such a hypothesis. Since initial conditions are unknown a priori, we take broad prior distributions, which are log-normal with standard deviation one half of the mean. The prior mean values were chosen based on preliminary computations, to obtain reasonable agreement with deaths in the first few weeks. Denoting these mean values by μ we take $\mu_\kappa = 5 \times 10^{-4}$ and for the oldest cohort $(\mu_E, \mu_A, \mu_{I^1}, \mu_{I^2}, \mu_{I^3}) = (2000, 1200, 300, 60, 40)$, see also Fig. 12 below.

3. Contact matrices

The contact matrices for C^P and C^F model variants are based on [48, 49], as we now explain. On general grounds, one expects contacts to obey a *reciprocal relation*: the matrix \mathbf{Q} with elements

$$Q_{ij} = N_i C_{ij} \quad (\text{C4})$$

should be symmetric, $Q_{ij} = Q_{ji}$.

For C^P , the contact matrix is taken from [48], by summing the contributions from home/work/school/other. It is notable (see for example Fig. 1) that the data do not satisfy (C4), this can be traced back to the reporting of contacts by the participants of [50].

For C^F , the data in [49] is provided as a (non-normalised) estimate of \mathbf{Q} , based on n_Q single-year age cohorts. As for C^P , we sum the contributions from different environments to obtain a single matrix. Let \mathcal{A}_i be the set of single-year age cohorts corresponding to the (5-year) cohort i , and denote the reported estimate of \mathbf{Q}

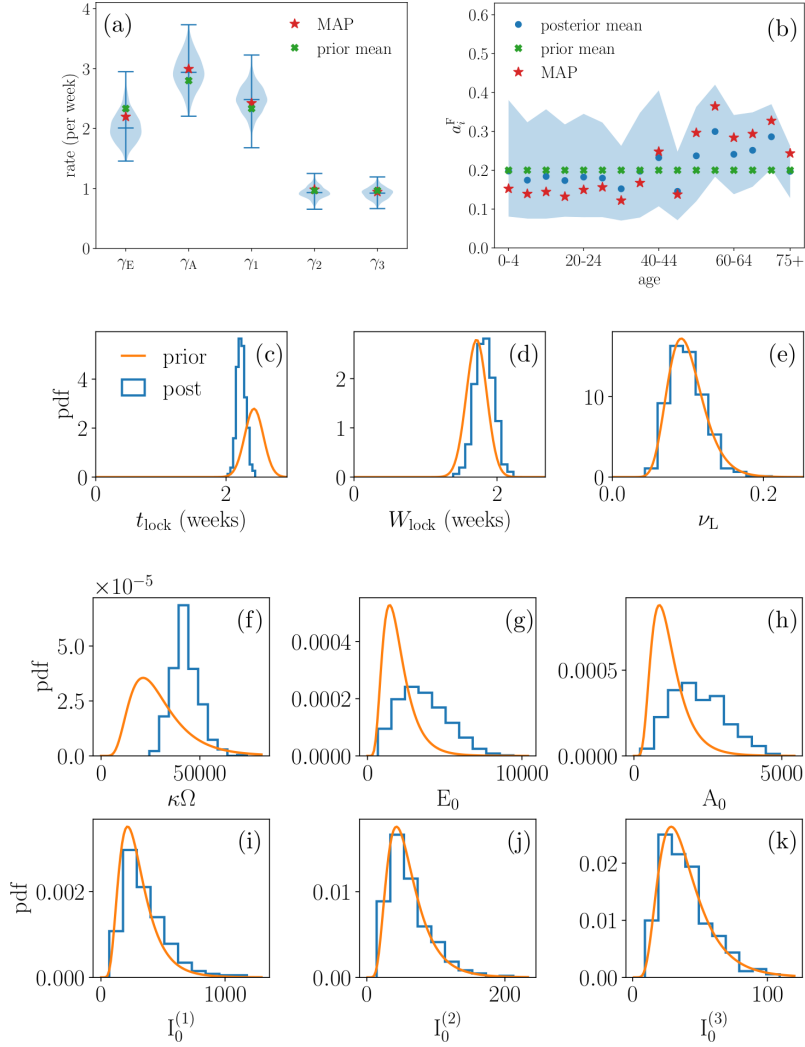


FIG. 12: Posterior for parameters, C^F model variant with step-like-NPI. (a) γ parameters, the violin plots are based on kernel density estimates. (b) a_i^F parameters, the shading is 5th to 95th percentile of the posterior. (c,d,e) prior and posterior distributions of lockdown parameters t_{lock} , W_{lock} and late-stage infectivity parameter ν_L . (f-k) prior and posterior distributions of initial condition parameters, specifically the coefficient κ of the leading mode, and the individual compartment populations for the oldest (75+) cohort.

by Q^0 . Then we take

$$C_{ij} = \frac{\Omega}{\chi N_i} \sum_{p \in \mathcal{A}_i} \sum_{q \in \mathcal{A}_j} Q_{pq}^0 \quad (\text{C5})$$

The constant χ is included because Q^0 is not normalised, we take $\chi = 3Mn_Q$ so that the typical numbers of contacts are comparable with [48]. This scaling is somewhat arbitrary but errors/uncertainties in this factor can be compensated by rescaling the β parameters of the model. The matrix Q^0 is symmetric so the resulting contact matrices obey (C4).

4. Additional results

This Section shows additional results from the inference methodology.

We have emphasised that our Bayesian analysis accounts for all sources of uncertainty in the model, including parameter uncertainty, and the stochasticity inherent in the compartment model. As a direct measure of this stochasticity, Fig. 11 shows a conditional nowcast, as defined in Sec. IV B. We show results summed over age cohorts, and for one representative cohort. These results illustrate the fluctuations that are captured by the functional CLT. For the summed data, the fluctuations are small, consistent with the relatively large numbers of individuals. At the level of specific cohorts, the fluctuations are significant.

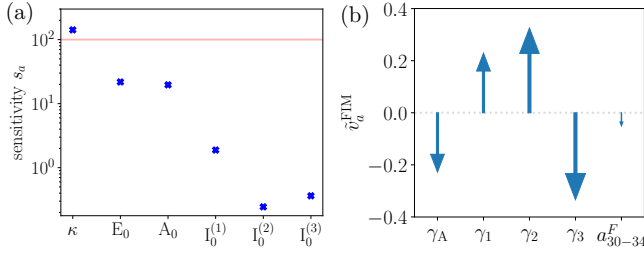


FIG. 13: (a) Sensitivities for the parameters determining initial conditions. (b) Soft mode of the FIM, showing the 5 largest \tilde{v}_a^{FIM} among the model parameters (we have excluded in this case parameters relevant for initial conditions). This mode illustrates that the model behaviour (and hence the likelihood) is almost unchanged if one increases the parameters γ_1, γ_2 and simultaneously reduces γ_A, γ_3 . Other model parameters have small contributions to this mode, as illustrated by the a_i^{F} parameter, which is the next largest element in magnitude.

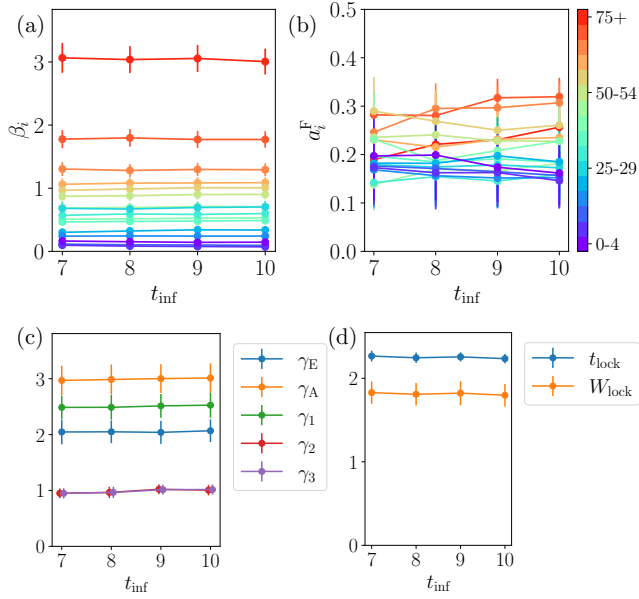


FIG. 14: Dependence of inferred parameters on time used for inference, see also Fig. 9. Plots show posterior mean with error bars showing posterior standard deviation. (C^{F} model variant, NPI-with-easing.)

Fig. 12 shows the posterior distributions of parameters for the C^{F} model with step-like NPI. This complements Fig. 4(b) of the main text where similar results are shown for the parameter β . In most cases, the posterior distributions overlap strongly with the priors, we

note however that the parameters have significant correlations under the posterior, which are not apparent here since we only show the marginals for individual variables. (For example, the initial rate of epidemic growth depends on a particular combination of the γ and β parameters; this growth rate is tightly constrained by the data, even if individual γ and β parameters remain uncertain.)

For the C^{F} model variant with step-like-NPI, we evaluated the FIM at the MAP parameters. Hence (i) we gain understanding of how sensitive our model is expected to be to small parameter perturbations and (ii) we understand whether there are soft directions along which the likelihood depends weakly on the parameters. The sensitivities for model parameters are discussed in Section VIB, see Fig. 5. There are corresponding sensitivities for the parameters that determine the initial condition, see Fig. 13(a). The parameter κ is sensitive to the data, as expected since it determines the size of the epidemic at early times.

The soft modes of the likelihood are determined by the eigenvalues and eigenvectors of the FIM. The eigenvectors corresponding to small eigenvalues define directions in which the likelihood is expected to change very little. Let \mathbf{v}^{FIM} be an eigenvector of the FIM \mathcal{I} with a small eigenvalue – its elements correspond to differences of the parameters θ from their MAP values. It is convenient to normalise these as fractional changes with respect to the MAP by defining a vector $\tilde{\mathbf{v}}^{\text{FIM}}$ with elements

$$\tilde{v}_a^{\text{FIM}} = \frac{1}{\theta_a^*} v_a^{\text{FIM}} \quad (\text{C6})$$

which is normalised such that $\sum_a |\tilde{v}_a^{\text{FIM}}|^2 = 1$. Hence large values of \tilde{v}_a^{FIM} indicate parameters that are significantly affected by the soft mode.

An example is given in Fig. 13(b). If one increases γ_A and reduces γ_1 appropriately, the result is a model with the same (mean) infectious period. A similar effect is obtained by increasing γ_2 and reducing γ_3 . Due to these degenerate directions in the parameter space, a pure maximum likelihood estimation (MLE) approach to inference of any model displaying soft modes potentially leads to wrong results. Bayesian inference on the other hand has the natural ability to remove soft modes by virtue of the additional information provided by priors.

Finally we consider the effects of the inference window. To complement Figs. 8 and 9, we show in Fig. 14 the dependence of inferred parameters on the time period used for inference (Fig. 9 shows similar results for the parameters r, ν_{L} .) Most parameters depend weakly on the time window, which indicates a robust forecast.

[1] N. M. Ferguson *et al.*, Imperial College COVID-19 Response Team Report 9, <http://doi.org/10.25561/77482> (2020).

[2] R. N. Thompson, T. D. Hollingsworth, V. Isham, D. Arribas-Bel, B. Ashby, T. Britton, P. Challenor, L. H. K. Chappell, H. Clapham, N. J. Cunniffe, A. P.

- Dawid, C. A. Donnelly, R. M. Eggo, S. Funk, N. Gilbert, P. Glendinning, J. R. Gog, W. S. Hart, H. Heesterbeek, T. House, M. Keeling, I. Z. Kiss, M. E. Kretzschmar, A. L. Lloyd, E. S. McBryde, J. M. McCaw, T. J. McKinley, J. C. Miller, M. Morris, P. D. O'Neill, K. V. Parag, C. A. B. Pearson, L. Pellis, J. R. C. Pulliam, J. V. Ross, G. S. Tomba, B. W. Silverman, C. J. Struchiner, M. J. Tildesley, P. Trapman, C. R. Webb, D. Mollison, and O. Restif, *Proc. Roy. Soc. B: Bio. Sci.* **287**, 20201405 (2020).
- [3] K. Prem, Y. Liu, T. W. Russell, A. J. Kucharski, R. M. Eggo, N. Davies, S. Flasche, S. Clifford, C. A. B. Pearson, J. D. Munday, S. Abbott, H. Gibbs, A. Rosello, B. J. Quilty, T. Jombart, F. Sun, C. Diamond, A. Gimma, K. van Zandvoort, S. Funk, C. I. Jarvis, W. J. Edmunds, N. I. Bosse, J. Hellewell, M. Jit, and P. Klepac, *The Lancet Public Health* **5**, e261 (2020).
- [4] N. G. Davies, A. J. Kucharski, R. M. Eggo, A. Gimma, W. J. Edmunds, T. Jombart, K. O'Reilly, A. Endo, J. Hellewell, E. S. Nightingale, B. J. Quilty, C. I. Jarvis, T. W. Russell, P. Klepac, N. I. Bosse, S. Funk, S. Abbott, G. F. Medley, H. Gibbs, C. A. B. Pearson, S. Flasche, M. Jit, S. Clifford, K. Prem, C. Diamond, J. Emery, A. K. Deol, S. R. Procter, K. van Zandvoort, Y. F. Sun, J. D. Munday, A. Rosello, M. Auzenberg, G. Knight, R. M. G. J. Houben, and Y. Liu, *The Lancet Public Health* **5**, e375 (2020).
- [5] S. M. Kissler, C. Tedijanto, E. Goldstein, Y. H. Grad, and M. Lipsitch, *Science* **368**, 860 (2020).
- [6] R. Singh and R. Adhikari, *arXiv preprint arXiv:2003.12055* (2020).
- [7] R. Verity, L. C. Okell, I. Dorigatti, P. Winskill, C. Whitaker, N. Imai, G. Cuomo-Dannenburg, H. Thompson, P. G. T. Walker, H. Fu, A. Dighe, J. T. Griffin, M. Baguelin, S. Bhatia, A. Boonyasiri, A. Cori, Z. Cucunubá, R. FitzJohn, K. Gaythorpe, W. Green, A. Hamlet, W. Hinsley, D. Laydon, G. Nedjati-Gilani, S. Riley, S. van Elsland, E. Volz, H. Wang, Y. Wang, X. Xi, C. A. Donnelly, A. C. Ghani, and N. M. Ferguson, *The Lancet Infectious Diseases* **20**, 669 (2020).
- [8] P. J. Birrell, J. Blake, E. van Leeuwen, PHE modelling cell, N. Gent, and D. De Angelis, *medRxiv:2020.08.24.20180737* (2020).
- [9] N. G. Davies, P. Klepac, Y. Liu, K. Prem, M. Jit, C. A. B. Pearson, B. J. Quilty, A. J. Kucharski, H. Gibbs, S. Clifford, A. Gimma, K. van Zandvoort, J. D. Munday, C. Diamond, W. J. Edmunds, R. M. G. J. Houben, J. Hellewell, T. W. Russell, S. Abbott, S. Funk, N. I. Bosse, Y. F. Sun, S. Flasche, A. Rosello, C. I. Jarvis, R. M. Eggo, and CMMID COVID-19 working group, *Nature Medicine* **26**, 1205 (2020).
- [10] R. Adhikari *et al.*, *arXiv:2005.09625* (2020).
- [11] K. J. Friston *et al.*, *arXiv:2004.04463* (2020).
- [12] N. T. J. Bailey, *The Mathematical Theory of Infectious Diseases and its Applications* (Charles Griffin & Company Ltd, High Wycombe, UK, 1975).
- [13] O. Diekmann, J. A. P. Heesterbeek, and M. G. Roberts, *J. Royal Soc. Int.* **7**, 873 (2010).
- [14] M. J. Keeling and P. Rohani, *Modeling Infectious Diseases in Humans and Animals* (Princeton University Press, 2011).
- [15] P. J. Birrell, X.-S. Zhang, R. G. Pebody, N. J. Gay, and D. De Angelis, *Scientific Reports* **6**, 29004 (2016).
- [16] H. Jeffreys, *The Theory of Probability* (Oxford University Press, Oxford, 1939).
- [17] A. Zellner, *An Introduction to Bayesian Inference in Econometrics* (John Wiley and Sons, New York, 1996).
- [18] D. J. C. MacKay, *Information Theory, Inference and Learning Algorithms* (Cambridge University Press, 2003).
- [19] P. D. O'Neill and G. O. Roberts, *J. Roy. Stat. Soc.: Series A* **162**, 121 (1999).
- [20] A. Chatzilela, E. van Leeuwen, O. Ratmann, M. Baguelin, and N. Demiris, *Epidemics* **29**, 100367 (2019).
- [21] J. Ross, T. Taimre, and P. Pollett, *Theoretical Population Biology* **70**, 498 (2006).
- [22] J. Ross, D. Pagendam, and P. Pollett, *Theoretical Population Biology* **75**, 123 (2009).
- [23] X. Xu, T. Kypraios, and P. D. O'Neill, *Biostatistics* **17**, 619 (2016).
- [24] E. Buckingham-Jeffery, V. Isham, and T. House, *Math. Biosci.* **301**, 111 (2018).
- [25] S. C. Leite and R. J. Williams, *Ann. Appl. Prob.* **29**, 1541 (2019).
- [26] <https://github.com/rajeshrinet/pyross>.
- [27] R. E. Kass and A. E. Raftery, *J. Am. Stat. Assoc.* **90**, 773 (1995).
- [28] A. E. Raftery, *Sociological methodology* **25**, 111 (1995).
- [29] D. J. C. MacKay, *Neural Comp.* **4**, 415 (1992).
- [30] K. M. Gamado, G. Streftaris, and S. Zachary, *J. Math. Biol.* **69**, 737 (2014).
- [31] J. F. C. Kingman, *J. Appl. Prob.* **6**, 1 (1969).
- [32] R. M. Anderson, B. Anderson, and R. M. May, *Infectious Diseases of Humans: Dynamics and Control* (Oxford university press, 1992).
- [33] D. R. McNeil and G. H. Weiss, *Biometrika* **64**, 553 (1977).
- [34] T. G. Kurtz, *J. Chem. Phys.* **57**, 2976 (1972).
- [35] T. G. Kurtz, *Approximation of Population Processes* (SIAM, 1981).
- [36] N. G. Van Kampen, *Stochastic processes in physics and chemistry* (Elsevier, 1992).
- [37] C. Gardiner, *Stochastic Methods: A Handbook for the Natural and Social Sciences*, 4th ed. (Springer-Verlag, Berlin/Heidelberg, 2009).
- [38] T. McKinley, A. R. Cook, and R. Deardon, *Int. J. Biostatistics* **5** (2009).
- [39] N. Hansen, Y. Akimoto, and P. Baudis, *CMA-ES/pycma on github*. <https://doi.org/10.5281/zenodo.2559634> (2019).
- [40] V. Costanza and J. H. Seinfeld, *J. Chem. Phys.* **74**, 3852 (1981).
- [41] R. Gunawan, Y. Cao, L. Petzold, and F. J. Doyle, *Biophys. J.* **88**, 2530–2540 (2005).
- [42] D. Foreman-Mackey, D. W. Hogg, D. Lang, and J. Goodman, *Pub. Astron. Soc. Pac.* **125**, 306 (2013), <https://github.com/dfm/emcee>.
- [43] D. T. Gillespie, *J. Phys. Chem.* **81**, 2340 (1977).
- [44] Y. Cao, D. T. Gillespie, and L. R. Petzold, *J. Chem. Phys.* **124**, 044109 (2006).
- [45] <https://www.ons.gov.uk/peoplepopulationandcommunity/birthsdeathsandmarriages/deaths/datasets/weeklyprovisionalfiguresondeathsregisteredinenglandandwales> (2020).
- [46] F. Riccardo *et al.*, *medrxiv:2020.04.08.20056861v1* (2020).
- [47] <https://www.google.com/covid19/mobility/> (2020).
- [48] K. Prem, A. R. Cook, and M. Jit, *PLoS Comp. Biol.* **13**, e1005697 (2017).

- [49] L. Fumanelli, M. Ajelli, P. Manfredi, A. Vespignani, and S. Merler, PLOS Comp. Biol. **8**, e1002673 (2012).
- [50] J. Mossong, N. Hens, M. Jit, P. Beutels, K. Auranen, R. Mikolajczyk, M. Massari, S. Salmaso, G. S. Tomba, J. Wallinga, J. Heijne, M. Sadkowska-Todys, M. Rosinska, and W. J. Edmunds, PLOS Medicine **5**, e74 (2008).
- [51] L. Malago and G. Pistone, in *Proceedings of the 2015 ACM Conference on Foundations of Genetic Algorithms XIII - FOGA 15* (ACM Press, 2015) p. 150–162.
- [52] A. Gelman and X.-L. Meng, Stat. Sci. **13**, 163 (1998).
- [53] D. Frenkel and B. Smit, *Understanding Molecular Simulation: From Algorithms to Applications* (Elsevier, 2001).
- [54] J. Skilling, Bayesian Anal. **1**, 833 (2006).
- [55] Y. M. Bar-On, R. Sender, A. I. Flamholz, R. Phillips, and R. Milo, arXiv:2006.01283 (2020).